

Reliable calculations of nuclear binding energies by the Gaussian process of machine learning*

Ziyi Yuan,¹ Dong Bai,² Zhen Wang,¹ and Zhongzhou Ren^{1,3,†}

¹*School of Physics Science and Engineering, Tongji University, Shanghai 200092, China*

²*College of Science, Hohai University, Nanjing 211100, Jiangsu, China*

³*Key Laboratory of Advanced Micro-Structure Materials, Ministry of Education, Shanghai 200092, China*

Reliable calculations of nuclear binding energies are crucial for advancing the research of nuclear physics. Machine learning provides an innovative approach to exploring complex physical problems. In this study, the nuclear binding energies are modeled directly using a machine-learning method called the Gaussian process. First, the binding energies for 2238 nuclei with $Z > 20$ and $N > 20$ are calculated using the Gaussian process in a physically motivated feature space, yielding an average deviation of 0.046 MeV and a standard deviation of 0.066 MeV. The results show the good learning ability of the Gaussian process in the studies of binding energies. Then, the predictive power of the Gaussian process is studied by calculating the binding energies for 108 nuclei newly included in AME2020. The theoretical results are in good agreement with the experimental data, reflecting the good predictive power of the Gaussian process. Moreover, the α -decay energies for 1169 nuclei with $50 \leq Z \leq 110$ are derived from the theoretical binding energies calculated using the Gaussian process. The average deviation and the standard deviation are, respectively, 0.047 MeV and 0.070 MeV. Noticeably, the calculated α -decay energies for the two new isotopes ^{204}Ac [M. H. Huang *et al.*, *Phys. Lett. B* **834**, 137484 (2022)] and ^{207}Th [H. B. Yang *et al.*, *Phys. Rev. C* **105**, L051302 (2022)] agree well with the latest experimental data. These results demonstrate that the Gaussian process is reliable for the calculations of nuclear binding energies. Finally, the α -decay properties of some unknown actinide nuclei are predicted using the Gaussian process. The predicted results can be useful guides for future research on binding energies and α -decay properties.

Keywords: nuclear binding energies, α decay, machine learning, Gaussian process

I. INTRODUCTION

Nuclear binding energies are important ground state properties that provide valuable information for probing nuclear structures [1–4] and serve as crucial inputs for some nuclear physics problems [5, 6]. For instance, binding energies play a key role in calculating the product cross sections for unknown nuclei using nuclear reaction models before synthesizing superheavy nuclei [7, 8]. They are also instrumental in identifying new nuclides in synthesis experiments of heavy and superheavy nuclei [9, 10] because α decay is one of the fundamental decay modes for most heavy and superheavy nuclei [11–13]. For α -emitters, there are two main α -decay observable properties, which are respectively α -decay energies and half-lives [14–18]. Thereinto, α -decay half-lives are strongly influenced by the α -decay energies, which can be calculated using the binding energies. Meanwhile, binding energies are also vital for calculating the properties of other radioactive decay modes, such as two-proton radioactivity [19] and heavy-cluster radioactivity [20]. Furthermore, the accuracy of binding energies has a significant impact on nuclear astrophysics studies, including r -process [21, 22], rp -process [23, 24], and the properties of neutron stars [25, 26]. Therefore, it is necessary to explore reliable theoretical models to calculate and predict the binding energies more accurately.

With the advancements in experimental nuclear physics facilities, binding energies of more than two thousand nuclei have been measured to date [27]. The accumulated experimental data provide a foundation for the development of theoretical models. In the past few years, numerous theoretical models and formulas have been proposed to calculate binding energies, including the Bethe-Weizsäcker formula [28, 29], the Thomas-Fermi (TF) model [30], the Hartree-Fock-Bogoliubov mean field model [31], and the finite-range drop model (FRDM) [32]. The theoretical binding energies calculated using these models and formulas are in good agreement with the experimental data. In Ref. [8], an improved binding-energy formula was proposed by incorporating additional physical terms into the standard Bethe-Weizsäcker formula, which consists of the shell effect and the neutron-proton correlations. The binding energies and α -decay energies can be well reproduced using this improved formula for heavy and superheavy nuclei with $Z \geq 90$ and $N \geq 140$. Although these current traditional models can provide theoretical guidance for studying binding energies, it is still worth exploring other models to provide more accurate calculations and predictions for future investigations of binding energies.

Machine learning has been widely used across many fields [33–38], as it can learn useful information from known systems and predict unknown properties within the same system using the obtained information. In the last decade, nuclear properties have been studied using various machine-learning methods based on available physical knowledge, including nuclear masses [39–41], nuclear charge radii [42], α -decay properties [43], and β -decay properties [44]. These nuclear properties can be well reproduced using machine learning. Recently, a new Bayesian machine learning mass model has been proposed [45], which can reproduce nuclear masses with the high accuracy required for the studies of r -process. As

* Supported by the National Key R&D Program of China (Contract No. 2023YFA1606503), and by the National Natural Science Foundation of China (Grants No. 12035011, No. 11975167, No. 11947211, No. 11905103, No. 11881240623, and No. 11961141003).

† Corresponding author, Zhongzhou.Ren@tongji.edu.cn.

one of the popular machine-learning methods, the Gaussian process is a powerful nonparametric model, which is expected to model any distribution of the objectives [46]. Owing to its excellent flexibility in data modeling, the Gaussian process has been frequently applied in various studies [47, 48]. Notably, the Gaussian process can provide not only the theoretical values of the objectives but also the distribution of the calculated results, contributing to the visualization of the theoretical uncertainties [49]. Recently, the Gaussian process has been successfully exploited to predict the α -decay energies and half-lives of actinide nuclei [50]. Inspired by these previous works, it is of great interest to explore the reliability of the Gaussian process in the calculations of binding energies.

In this work, the Gaussian process has been extended to study the binding energies by directly modeling the experimental binding energies. The remainder of this paper is given as follows. In Sec. II, the theoretical framework, consisting of the Gaussian process with the modified kernel function and the physically motivated feature space, is provided. In Sec. III, the theoretical binding energies calculated using the Gaussian process are shown and discussed. Furthermore, the α -decay properties are reproduced and predicted based on the calculated binding energies. Finally, a comprehensive summary is presented in Sec. IV.

II. THEORETICAL FRAMEWORK

In the present work, the binding energy for a nucleus is considered as a realistic observation $B_p = b_p + \tilde{\delta}$ with noise $\tilde{\delta} \sim \mathcal{N}(0, \sigma_b^2)$. Here, $b_p = b(\mathbf{x}_p)$ is a latent function that denotes the noise-free binding energy for the p th nucleus \mathbf{x}_p [51]. B_p denotes the realistic binding energy, and $\tilde{\delta}$ is an independently identically distributed Gaussian noise. Given a set of n nuclei with known binding energies into a training set $(\mathbf{x}_p, B_p)_{p=1}^n$, we aim to model the underlying physical relationship between each nucleus and its binding energy using the Gaussian process. Within the framework of the Gaussian process, the values of latent function $\mathbf{b} = (b_1, b_2, \dots, b_n)^T = (b(\mathbf{x}_1), b(\mathbf{x}_2), \dots, b(\mathbf{x}_n))^T$ are modeled by a joint Gaussian distribution, characterized by the values of a mean function $(m(\mathbf{x}_1), m(\mathbf{x}_2), \dots, m(\mathbf{x}_n))^T$ and the matrix of a covariance function $[k(\mathbf{x}_p, \mathbf{x}_q)]_{n \times n}$ [46]. Therefore, the Gaussian process can be generally denoted as $b(\mathbf{x}_p) \sim \mathcal{GP}(m(\mathbf{x}_p), k(\mathbf{x}_p, \mathbf{x}_q))$. The mean function $m(\mathbf{x}_p)$ is often set as zero because of the lack of prior knowledge. The so-called kernel function $k(\mathbf{x}_p, \mathbf{x}_q)$ can be written as a function of $|\mathbf{x}_p - \mathbf{x}_q|$, which is crucial for describing the similarities between pairs of nuclei. For the studies of binding energies, we choose a composite kernel function written as

$$k(\mathbf{x}_p, \mathbf{x}_q) = \eta_b^2 \left[\left(1 + \frac{\sqrt{3}r_b}{l_b} \right) \exp \left(-\frac{\sqrt{3}r_b}{l_b} \right) + \left(1 + \frac{r_b^2}{2\alpha_b d_b^2} \right)^{-\alpha_b} \right] \quad (1)$$

with $r_b = |\mathbf{x}_p - \mathbf{x}_q|$. The modified kernel function is a linear combination of two widely used kernel functions, which are the Matérn kernel function and the Rational Quadratic ker-

nel function, respectively. Here, η_b , l_b , α_b , and d_b are four hyperparameters of the Gaussian process. l_b , α_b , and d_b can capture the relevant range of the binding energies for pairs of nuclei, and η_b is able to describe the correlation intensity between them. For the realistic binding energy B_p , the covariance function becomes $k(\mathbf{x}_p, \mathbf{x}_q) \rightarrow k(\mathbf{x}_p, \mathbf{x}_q) + \sigma_b^2 \delta_{pq}$. δ_{pq} is a Kronecker delta where $\delta_{pq} = 1$ for $p = q$ and $\delta_{pq} = 0$ for $p \neq q$. When describing a number of nuclei $\mathbf{X} = (\mathbf{x}_1, \mathbf{x}_2, \dots, \mathbf{x}_n)^T$, the binding energies $\mathbf{B} = (B_1, B_2, \dots, B_n)^T$ are expressed as $\mathbf{B} \sim \mathcal{GP}(\mathbf{0}, \mathbf{K}(\mathbf{X}, \mathbf{X}) + \sigma_b^2 \mathbf{I})$, where \mathbf{I} is a diagonal matrix.

The central interest of this work is to predict unknown binding energies based on the knowledge learned from the training set using the Gaussian process. When predicting unknown binding energies for nuclei \mathbf{X}_* with the training set $\mathcal{D} = (\mathbf{x}_p, B_p)_{p=1}^n$, the joint Gaussian distribution of the training outputs \mathbf{B} and the predicted outputs \mathbf{b}_* can be written as [46]

$$\begin{bmatrix} \mathbf{B} \\ \mathbf{b}_* \end{bmatrix} \sim \mathcal{N} \left(\mathbf{0}, \begin{bmatrix} \mathbf{K}(\mathbf{X}, \mathbf{X}) + \sigma_b^2 \mathbf{I} & \mathbf{K}(\mathbf{X}, \mathbf{X}_*) \\ \mathbf{K}(\mathbf{X}_*, \mathbf{X}) & \mathbf{K}(\mathbf{X}_*, \mathbf{X}_*) \end{bmatrix} \right) \quad (2)$$

For n_* predicted nuclei, $\mathbf{K}(\mathbf{X}, \mathbf{X})$, $\mathbf{K}(\mathbf{X}, \mathbf{X}_*)$, $\mathbf{K}(\mathbf{X}_*, \mathbf{X})$, and $\mathbf{K}(\mathbf{X}_*, \mathbf{X}_*)$, respectively, denote $n \times n$, $n \times n_*$, $n_* \times n$, and $n_* \times n_*$ matrix evaluated at all pairs of training and predicted points. By conditioning the joint Gaussian distribution, the crucial predicted expressions for the Gaussian process are $\mathbf{b}_* | \mathcal{D}, \mathbf{X}_* \sim \mathcal{N}(\mathbf{b}_*, \text{cov}(\mathbf{b}_*))$, where

$$\begin{aligned} \mathbf{b}_* &= \mathbf{K}(\mathbf{X}_*, \mathbf{X}) [\mathbf{K}(\mathbf{X}, \mathbf{X}) + \sigma_b^2 \mathbf{I}]^{-1} \mathbf{B}, \\ \text{cov}(\mathbf{b}_*) &= \mathbf{K}(\mathbf{X}_*, \mathbf{X}_*) - \mathbf{K}(\mathbf{X}_*, \mathbf{X}) [\mathbf{K}(\mathbf{X}, \mathbf{X}) + \sigma_b^2 \mathbf{I}]^{-1} \mathbf{K}(\mathbf{X}, \mathbf{X}_*). \end{aligned} \quad (3)$$

Here, the values of \mathbf{b}_* give the predicted binding energies for unknown nuclei. The variances of the predicted binding energies can be calculated by adding the noise variance σ_b^2 to the predictive variance given by $\text{cov}(\mathbf{b}_*)$.

As mentioned above, each nucleus is described by \mathbf{x}_p , which is a vector of physical features determining the description of the corresponding binding energy. In the present work, our goal is to obtain good descriptions of the binding energies using the Gaussian process with as simple physical information as possible. Hence, we construct a physical feature space with nine features, where $\mathbf{x}_p = (A_p, A_p^{2/3}, Z_p^2 A_p^{-1/3}, (A_p/2 - Z_p)^2 / A_p, A_p^{-1/2}, \delta_p, |N_p - Z_p| / A_p, \pi_p, v_p)$. Here, A , Z , and N denote the mass, proton, and neutron numbers, respectively. The first six features are based on the Bethe-Weizsäcker formula [7, 28, 29, 52, 53]. A is introduced to model the proportional relationship between the binding energies and the nuclear volume, reflecting the saturation of nuclear force. $A^{2/3}$ is provided since the binding energies are expected to decrease on the nuclear surface. $Z^2 A^{-1/3}$ is used to describe the influence of the Coulomb interaction between protons. $(A/2 - Z)^2 / A$ is the symmetry term that approximately estimates the balance between N and Z . $A^{-1/2}$ and $\delta = [(-1)^N + (-1)^Z] / 2$ are used to describe the pairing energies with $\delta = 1, 0, -1$ for the even-even, odd- A , and odd-odd nuclei. $|N - Z| / A$ is from the Wigner term, which originates from the neutron-proton correlations [1, 8].

164 Additionally, π and v include the shell information, where
 165 π (v) is calculated using the numbers of protons (neutrons)
 166 away from the nearest proton (neutron) magic numbers [54].

167 The aforementioned theoretical framework implies that
 168 five hyperparameters need to be determined, which are η_b , l_b ,
 169 α_b , d_b , and σ_b , respectively. These can be determined by op-
 170 timizing the marginal likelihood using the training data [46].

171 III. NUMERICAL RESULTS AND DISCUSSIONS

172 In this section, we present and discuss the theoretical re-
 173 sults of the nuclear binding energies calculated using the
 174 Gaussian process. First, we calculate the binding en-
 175 ergies for nuclei with $Z > 20$ and $N > 20$ to evaluate
 176 the learning ability of the Gaussian process. The training
 177 set chosen in this work contains 2238 nuclei with known
 178 binding energies taken from AME2020 [55]. Each nucleus
 179 in the training set is presented as (\mathbf{x}_p, B_p) , where $\mathbf{x}_p =$
 180 $(A_p, A_p^{2/3}, Z_p^2 A_p^{-1/3}, (A_p/2 - Z_p)^2/A_p, A_p^{-1/2}, \delta_p, |N_p -$
 181 $Z_p|/A_p, \pi_p, v_p)$ and $B_p = B_p^{\text{Expt.}}$. After the training pro-
 182 cess, the hyperparameters are determined as $\eta_b = 1.814 \times$
 183 $10^4 \text{ MeV}^{1/2}$, $l_b = 1.821 \times 10^4$, $\alpha_b = 1937.218$, $d_b =$
 184 414.771 , and $\sigma_b = 0.093 \text{ MeV}^{1/2}$. The larger value of η_b in-
 185 dicates a stronger dependence between pairs of nuclei. Mean-
 186 while, the larger values of l_b , α_b , and d_b result in a relatively
 187 larger correlation range, which means that the change of bind-
 188 ing energies is comparatively smoother. Moreover, they also
 189 assist in avoiding the rapid growth of the error bars of the
 190 binding energies for nuclei away from the training data [46].

191 After the hyperparameters have been determined, the bind-
 192 ing energies can be calculated using the Gaussian process. To
 193 test the accuracy of the calculated results, we calculate the ab-
 194 solute value of the deviation between the experimental result
 195 and the theoretical one for each nucleus, defined by

$$196 \quad |\Delta_B| = |B_p^{\text{Expt.}} - B_p^{\text{Theo.}}|. \quad (4)$$

197 Here, $B_p^{\text{Expt.}}$ and $B_p^{\text{Theo.}}$ denote the experimental binding en-
 198 ergy and theoretical result calculated using the Gaussian pro-
 199 cess for the p th nucleus, respectively. The numerical results
 200 show that all absolute values of the deviations are smaller than
 201 0.423 MeV, indicating a small global deviation. We show the
 202 corresponding results in Fig. 1, in which the x- and y-axis in-
 203 dicate the neutron and proton numbers, respectively. The red
 204 squares depict the absolute values of the deviations, where
 205 darker colors are associated with larger deviations. The trans-
 206 verse and vertical dotted lines present $N = 28, 50, 82, 126$
 207 and $Z = 28, 50, 82$, respectively. It can be seen clearly from
 208 Fig. 1 that the colors of most squares are lighter, reflecting
 209 that the deviations for most nuclei are below 0.1 MeV. Addi-
 210 tionally, the binding energies for nuclei near the shell closure
 211 are also well reproduced using the Gaussian process. Next,
 212 we calculate the average deviation

$$213 \quad \langle \sigma_B \rangle = \frac{1}{\tilde{n}_B} \sum_{p=1}^{\tilde{n}_B} |B_p^{\text{Expt.}} - B_p^{\text{Theo.}}| \quad (5)$$

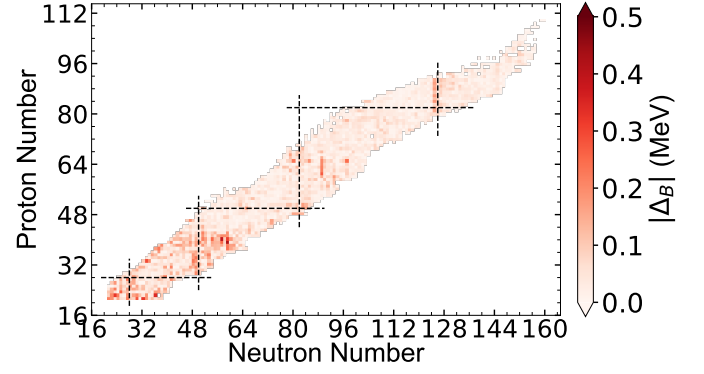


Fig. 1. The absolute values of deviations between experimen-
 tal binding energies and the theoretical results calculated using the
 Gaussian process across the nuclear chart. The darker colors indi-
 cate larger deviations of binding energies. Numerically, the largest
 absolute value of the deviations is $|\Delta_B| = 0.423 \text{ MeV}$.

214 and the standard deviation

$$215 \quad \sqrt{\sigma_B^2} = \sqrt{\frac{1}{\tilde{n}_B} \sum_{p=1}^{\tilde{n}_B} (B_p^{\text{Expt.}} - B_p^{\text{Theo.}})^2} \quad (6)$$

216 of the theoretical binding energies calculated using the Gaus-
 217 sian process for nuclei with $Z > 20$ and $N > 20$. Here,
 218 \tilde{n}_B denotes the number of nuclei included in the calcula-
 219 tions. The numerical values are $\langle \sigma_B \rangle = 0.046 \text{ MeV}$ and
 220 $\sqrt{\sigma_B^2} = 0.066 \text{ MeV}$, respectively. The small deviations
 221 show that the theoretical binding energies calculated using
 222 the Gaussian process with the modified kernel function in
 223 the physically motivated feature space are in good agreement
 224 with the experimental data. These results demonstrate the
 225 good learning ability of the Gaussian process in the studies
 226 of binding energies.

227 To further evaluate the learning ability and predictive
 228 power of the Gaussian process in the studies of binding en-
 229 ergies, we perform cross validation for the Gaussian process.
 230 In this work, we introduce the isotone-fold cross-validation
 231 that nuclei in each isotonic chain will be predicted using the
 232 Gaussian process based on the information provided by the
 233 remaining isotonic chains in the training set. The average de-
 234 viations and the standard deviations of the theoretical binding
 235 energies for nuclei in each isotonic chain are calculated, with
 236 results depicted in Fig. 2. For comparison, the average de-
 237 viations and the standard deviations of the binding energies cal-
 238 culated using the Bethe-Weizsäcker formula for each isotonic
 239 chain are also provided in Fig. 2. In Fig. 2(a) and Fig. 2(b),
 240 the red squares denote the average deviations and the standard
 241 deviations calculated using the Gaussian process for each iso-
 242 tonic chain, respectively. The blue circles present the average
 243 deviations and the standard deviations calculated using the
 244 Bethe-Weizsäcker formula for each isotonic chain separately.
 245 It is straightforward to see that the deviations given by the
 246 Gaussian process are quite small, which means that the cross-
 247 validation result is pretty good. In addition, we can find that
 248 the deviations are significantly reduced compared with those

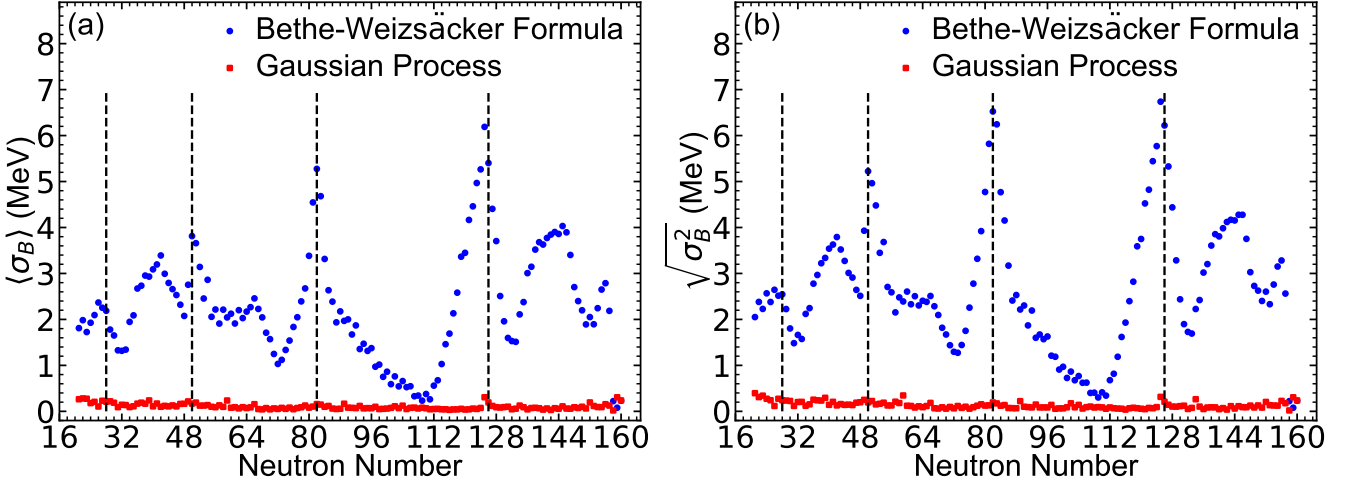


Fig. 2. The cross-validation results for nuclei in each isotopic chain calculated using the Gaussian process. In Fig. 2(a), the red squares and the blue circles depict the average deviations calculated using the Gaussian process and the Bethe-Weizsäcker formula, respectively. In Fig. 2(b), the red squares and the blue circles show the standard deviations calculated using the Gaussian process and the Bethe-Weizsäcker formula separately.

given by the Bethe-Weizsäcker formula. These results reflect the good learning ability and predictive power of the Gaussian process. Numerically, the total average deviation and standard deviation of the cross-validation for nuclei in the training set are $\langle \sigma_B \rangle = 0.100$ MeV and $\sqrt{\sigma_B^2} = 0.144$ MeV, respectively. The small deviations show that the predicted binding energies agree well with the experimental data, indicating that the binding energies can be well learned using the Gaussian process. Thus, we can conclude that the learning ability and predictive power of the Gaussian process are reliable for studying the binding energies.

Then, we further test the predictive power of the Gaussian process by calculating the binding energies for nuclei that are present in AME2020 but not in AME2012 using the Gaussian process. To perform this calculation, the training set is chosen to include nuclei that are provided in both AME2012 and AME2020. Based on the training set, we predict the binding energies for 108 nuclei that are provided in AME2020 but not in AME2012 using the Gaussian process. The theoretical average deviation and standard deviation for these nuclei are $\langle \sigma_B \rangle = 0.216$ MeV and $\sqrt{\sigma_B^2} = 0.304$ MeV, respectively. These deviations are acceptable results in the calculations of binding energies, verifying that the predicted power of the Gaussian process is commendable. Therefore, based on these theoretical results, it can be concluded that the Gaussian process is a reliable model for the studies of nuclear binding energies.

Next, we would like to calculate and discuss the theoretical results calculated using the Gaussian process with different kernel functions and physical feature spaces. First, we calculate the binding energies using the Gaussian process with the Matérn kernel function and the Rational Quadratic kernel function, respectively. The corresponding deviations of the binding energies for 2238 nuclei are $(\langle \sigma_B \rangle, \sqrt{\sigma_B^2}) = (0.059, 0.076)$ MeV for the Matérn ker-

nel function and $(\langle \sigma_B \rangle, \sqrt{\sigma_B^2}) = (0.121, 0.166)$ MeV for the Rational Quadratic kernel function, respectively. The deviations for 108 new nuclei are $(\langle \sigma_B \rangle, \sqrt{\sigma_B^2}) = (0.278, 0.415)$ MeV for the Matérn kernel function and $(\langle \sigma_B \rangle, \sqrt{\sigma_B^2}) = (0.193, 0.249)$ MeV for the Rational Quadratic kernel function separately. Comparing with the deviations $(\langle \sigma_B \rangle, \sqrt{\sigma_B^2}) = (0.046, 0.066)$ MeV for 2238 nuclei and $(\langle \sigma_B \rangle, \sqrt{\sigma_B^2}) = (0.216, 0.304)$ MeV for 108 new nuclei calculated using the composite kernel function, it can be found that the deviations calculated with the composite kernel function are as small as those calculated using the Matérn kernel function for 2238 nuclei and show better results than those calculated using the Matérn kernel function for 108 new nuclei. The deviations calculated using the composite kernel function show results as good as those calculated using the Rational Quadratic kernel function for 108 new nuclei and are smaller than those calculated using the Rational Quadratic kernel function for 2238 nuclei. Therefore, the good interpolation power of the Gaussian process with the Matérn kernel function and extrapolation ability of the Gaussian process with the Rational Quadratic kernel function are inherited by the composite kernel function in the calculations of binding energies, which demonstrates that the modified kernel function is a good choice for the present work. Furthermore, we hope that the choice of the composite kernel function can provide a new idea for modeling other physical problems using the Gaussian process.

We continue to compare the average deviations and standard deviations for 108 new nuclei using the Gaussian process in different physical feature spaces. We first calculate the deviations for nuclei using the Gaussian process in the feature space consisting of six features taken from the Bethe-Weizsäcker formula, where the p th nucleus is described by $\mathbf{x}_p = (A_p, A_p^{2/3}, Z_p^2 A_p^{-1/3}, (A_p/2 -$

$Z_p)^2/A_p, A_p^{-1/2}, \delta_p)$. The theoretical deviations are
 $(\langle\sigma_B\rangle, \sqrt{\sigma_B^2}) = (0.437, 0.775)$ MeV. Then, we add the
 neutron-proton correlation and the shell information in the
 above feature space and compare the corresponding deviations.
 When the neutron-proton correlation is added in the
 feature space where $\mathbf{x}_p = (A_p, A_p^{2/3}, Z_p^2 A_p^{-1/3}, (A_p/2 -$
 $Z_p)^2/A_p, A_p^{-1/2}, \delta_p, |N_p - Z_p|/A_p)$, the deviations become
 $(\langle\sigma_B\rangle, \sqrt{\sigma_B^2}) = (0.398, 0.712)$ MeV. The reduction in the
 deviations shows that the neutron-proton correlation is necessary
 for calculating the binding energies. When the shell
 information is included in the feature space, where $\mathbf{x}_p =$
 $(A_p, A_p^{2/3}, Z_p^2 A_p^{-1/3}, (A_p/2 - Z_p)^2/A_p, A_p^{-1/2}, \delta_p, \pi_p, \nu_p)$,
 the deviations are $(\langle\sigma_B\rangle, \sqrt{\sigma_B^2}) = (0.236, 0.365)$ MeV. The
 results reflect that the introduced features π and ν provide
 useful shell information for nuclei in the calculations of binding
 energies. Furthermore, it can be observed that the above
 deviations are larger than those calculated in the feature space
 with nine features established in the present work, indicating
 that our choice of feature space is reasonable. Notably, the
 importance of the physically motivated feature space has also
 been studied in the Bayesian neural network and the probabilistic
 Mixture Density Network [39, 41]. The physical feature
 space established in the present work is first studied in the
 Gaussian process on the research of binding energies.
 It has been mentioned that the distribution of theoretical
 results can be provided by the Gaussian process. Here, we
 present the intervals of error bars for the theoretical results
 calculated in this work. The lengths of error bars at 95%
 confidence interval range from 0.213 MeV to 0.258 MeV in
 the studies of 2238 nuclei, while they range from 0.234 MeV
 to 4.022 MeV in the calculations of 108 new nuclei. These
 results show that the hyperparameters determined by the
 marginal likelihood are reasonable and that the theoretical
 binding energies calculated using the Gaussian process are
 reliable. Thus, we conclude that the Gaussian process with a
 modified kernel function and the physically motivated feature
 space is a reliable model for calculating binding energies.

Table 1: The theoretical α -decay energies calculated using the Gaussian process for some actinide nuclei. The first column denotes the actinide nuclei. The second and third columns list the experimental α -decay energies and the theoretical values calculated using the Gaussian process separately. The last column presents the deviations $\Delta Q_\alpha = Q_\alpha^{\text{Expt.}} - Q_\alpha^{\text{Theo.}}$. The experimental data for the new nuclides ^{204}Ac and ^{207}Th are taken from Ref. [57] and Ref. [10], respectively.

Nucl.	$Q_\alpha^{\text{Expt.}}$ (MeV)	$Q_\alpha^{\text{Theo.}}$ (MeV)	ΔQ_α (MeV)
^{204}Ac [57]	8.107	8.107	0.000
^{205}Ac	8.093	8.083	0.010
^{206}Ac	7.958	7.943	0.015
^{207}Ac	7.845	7.863	-0.018
^{208}Ac	7.729	7.736	-0.007
^{209}Ac	7.730	7.703	0.027
^{210}Ac	7.586	7.608	-0.022
^{211}Ac	7.568	7.569	-0.001

Table 1: (continued)

Nucl.	$Q_\alpha^{\text{Expt.}}$ (MeV)	$Q_\alpha^{\text{Theo.}}$ (MeV)	ΔQ_α (MeV)
^{212}Ac	7.540	7.490	0.050
^{213}Ac	7.498	7.491	0.007
^{214}Ac	7.352	7.531	-0.179
^{215}Ac	7.746	7.718	0.028
^{216}Ac	9.241	9.012	0.229
^{217}Ac	9.832	9.931	-0.099
^{218}Ac	9.384	9.437	-0.053
^{219}Ac	8.826	8.818	0.008
^{220}Ac	8.348	8.324	0.024
^{221}Ac	7.791	7.741	0.050
^{222}Ac	7.137	7.226	-0.089
^{223}Ac	6.783	6.761	0.022
^{224}Ac	6.327	6.318	0.009
^{225}Ac	5.935	5.924	0.011
^{226}Ac	5.506	5.483	0.023
^{227}Ac	5.042	5.115	-0.073
^{228}Ac	4.721	4.697	0.024
^{229}Ac	4.444	4.382	0.062
^{230}Ac	3.893	3.934	-0.041
^{231}Ac	3.655	3.679	-0.024
^{232}Ac	3.345	3.345	0.000
^{233}Ac	3.215	3.197	0.018
^{234}Ac	2.930	2.942	-0.012
^{235}Ac	2.852	2.886	-0.034
^{236}Ac	2.723	2.668	0.055
^{207}Th [10]	8.328	8.277	0.051
^{208}Th	8.202	8.210	-0.008
^{210}Th	8.069	8.065	0.004
^{211}Th	7.937	7.947	-0.010
^{212}Th	7.958	7.927	0.031
^{213}Th	7.837	7.817	0.020
^{214}Th	7.827	7.813	0.014
^{215}Th	7.665	7.840	-0.175
^{216}Th	8.072	8.056	0.016
^{217}Th	9.435	9.184	0.251
^{218}Th	9.849	9.971	-0.122
^{219}Th	9.506	9.531	-0.025
^{220}Th	8.973	8.994	-0.021
^{221}Th	8.625	8.595	0.030
^{222}Th	8.133	8.084	0.049
^{223}Th	7.567	7.656	-0.089
^{224}Th	7.299	7.275	0.024
^{225}Th	6.921	6.884	0.037

Table 1: (continued)

Nucl.	$Q_{\alpha}^{\text{Expt.}}$ (MeV)	$Q_{\alpha}^{\text{Theo.}}$ (MeV)	ΔQ_{α} (MeV)
²²⁶ Th	6.453	6.491	-0.038
²²⁷ Th	6.147	6.068	0.079
²²⁸ Th	5.520	5.598	-0.078
²²⁹ Th	5.168	5.124	0.044
²³⁰ Th	4.770	4.758	0.012
²³¹ Th	4.213	4.289	-0.076
²³² Th	4.082	4.052	0.030
²³³ Th	3.745	3.757	-0.012
²³⁴ Th	3.672	3.643	0.029
²³⁵ Th	3.376	3.406	-0.030
²³⁶ Th	3.333	3.344	-0.011
²³⁷ Th	3.196	3.146	0.050
²¹¹ Pa	8.481	8.467	0.014
²¹² Pa	8.411	8.418	-0.007
²¹³ Pa	8.384	8.354	0.030
²¹⁴ Pa	8.271	8.265	0.006
²¹⁵ Pa	8.236	8.212	0.024
²¹⁶ Pa	8.099	8.269	-0.170
²¹⁷ Pa	8.489	8.492	-0.003
²¹⁸ Pa	9.791	9.533	0.258
²¹⁹ Pa	10.128	10.233	-0.105
²²⁰ Pa	9.704	9.762	-0.058
²²¹ Pa	9.248	9.225	0.023
²²² Pa	8.789	8.784	0.005
²²³ Pa	8.343	8.270	0.073
²²⁴ Pa	7.694	7.788	-0.094
²²⁵ Pa	7.401	7.379	0.022
²²⁶ Pa	6.987	6.965	0.022
²²⁷ Pa	6.580	6.610	-0.030
²²⁸ Pa	6.265	6.226	0.039
²²⁹ Pa	5.835	5.866	-0.031
²³⁰ Pa	5.439	5.432	0.007
²³¹ Pa	5.150	5.102	0.048
²³² Pa	4.627	4.658	-0.031
²³³ Pa	4.375	4.403	-0.028
²³⁴ Pa	4.076	4.110	-0.034
²³⁵ Pa	4.101	4.035	0.066
²³⁶ Pa	3.755	3.810	-0.055
²³⁷ Pa	3.795	3.795	0.000
²³⁸ Pa	3.628	3.573	0.055
²¹⁵ U	8.588	8.569	0.019
²¹⁶ U	8.531	8.570	-0.039
²¹⁸ U	8.775	8.840	-0.065

Table 1: (continued)

Nucl.	$Q_{\alpha}^{\text{Expt.}}$ (MeV)	$Q_{\alpha}^{\text{Theo.}}$ (MeV)	ΔQ_{α} (MeV)
²¹⁹ U	9.950	9.780	0.170
²²¹ U	9.889	9.965	-0.076
²²² U	9.481	9.459	0.022
²²³ U	9.158	9.113	0.045
²²⁴ U	8.628	8.580	0.048
²²⁵ U	8.007	8.107	-0.100
²²⁶ U	7.701	7.662	0.039
²²⁷ U	7.235	7.230	0.005
²²⁸ U	6.800	6.828	-0.028
²²⁹ U	6.476	6.413	0.063
²³⁰ U	5.992	6.030	-0.038
²³¹ U	5.576	5.608	-0.032
²³² U	5.414	5.345	0.069
²³³ U	4.909	4.994	-0.085
²³⁴ U	4.858	4.860	-0.002
²³⁵ U	4.678	4.629	0.049
²³⁶ U	4.573	4.551	0.022
²³⁷ U	4.234	4.290	-0.056
²³⁸ U	4.270	4.273	-0.003
²³⁹ U	4.130	4.078	0.052
²⁴⁰ U	4.035	4.067	-0.032
²¹⁹ Np	9.207	9.238	-0.031
²²⁰ Np	10.226	10.100	0.126
²²² Np	10.200	10.222	-0.022
²²³ Np	9.650	9.664	-0.014
²²⁴ Np	9.329	9.323	0.006
²²⁵ Np	8.818	8.765	0.053
²²⁶ Np	8.328	8.363	-0.035
²²⁷ Np	7.816	7.847	-0.031
²²⁹ Np	7.020	7.061	-0.041
²³⁰ Np	6.778	6.757	0.021
²³¹ Np	6.368	6.338	0.030
²³³ Np	5.627	5.645	-0.018
²³⁴ Np	5.356	5.376	-0.020
²³⁵ Np	5.194	5.184	0.010
²³⁶ Np	5.007	5.021	-0.014
²³⁷ Np	4.957	4.908	0.049
²³⁸ Np	4.691	4.723	-0.032
²³⁹ Np	4.597	4.640	-0.043
²⁴⁰ Np	4.557	4.474	0.083
²⁴¹ Np	4.363	4.363	0.000
²⁴² Np	4.098	4.123	-0.025
²²⁸ Pu	7.940	7.910	0.030

Table 1: (continued)

Nucl.	$Q_{\alpha}^{\text{Expt.}}$ (MeV)	$Q_{\alpha}^{\text{Theo.}}$ (MeV)	ΔQ_{α} (MeV)
²²⁹ Pu	7.598	7.532	0.066
²³⁰ Pu	7.178	7.207	-0.029
²³¹ Pu	6.839	6.890	-0.051
²³² Pu	6.716	6.689	0.027
²³³ Pu	6.416	6.426	-0.010
²³⁴ Pu	6.310	6.261	0.049
²³⁵ Pu	5.951	6.011	-0.060
²³⁶ Pu	5.867	5.883	-0.016
²³⁷ Pu	5.748	5.697	0.051
²³⁸ Pu	5.593	5.555	0.038
²³⁹ Pu	5.245	5.332	-0.087
²⁴⁰ Pu	5.256	5.248	0.008
²⁴¹ Pu	5.140	5.094	0.046
²⁴² Pu	4.984	4.982	0.002
²⁴³ Pu	4.757	4.787	-0.030
²⁴⁴ Pu	4.666	4.661	0.005
²²⁹ Am	8.137	8.123	0.014
²³⁵ Am	6.576	6.622	-0.046
²³⁶ Am	6.256	6.378	-0.122
²³⁸ Am	6.042	6.038	0.004
²³⁹ Am	5.922	5.909	0.013
²⁴⁰ Am	5.707	5.731	-0.024
²⁴¹ Am	5.638	5.667	-0.029
²⁴² Am	5.589	5.519	0.070
²⁴³ Am	5.439	5.413	0.026
²⁴⁴ Am	5.138	5.207	-0.069
²⁴⁵ Am	5.160	5.152	0.008
²³³ Cm	7.473	7.518	-0.045
²³⁴ Cm	7.365	7.382	-0.017
²³⁶ Cm	7.067	7.041	0.026
²³⁷ Cm	6.770	6.815	-0.045
²³⁸ Cm	6.670	6.676	-0.006
²³⁹ Cm	6.540	6.498	0.042
²⁴⁰ Cm	6.398	6.396	0.002
²⁴¹ Cm	6.185	6.248	-0.063
²⁴² Cm	6.216	6.208	0.008
²⁴³ Cm	6.169	6.083	0.086
²⁴⁴ Cm	5.902	5.910	-0.008
²⁴⁵ Cm	5.624	5.657	-0.033
²⁴⁶ Cm	5.475	5.489	-0.014
²⁴⁷ Cm	5.354	5.311	0.043
²⁴⁸ Cm	5.162	5.207	-0.045
²⁴⁹ Cm	5.148	5.154	-0.006

Table 1: (continued)

Nucl.	$Q_{\alpha}^{\text{Expt.}}$ (MeV)	$Q_{\alpha}^{\text{Theo.}}$ (MeV)	ΔQ_{α} (MeV)
²⁵⁰ Cm	5.170	5.155	0.015
²³⁴ Bk	8.099	7.882	0.217
²⁴³ Bk	6.874	6.909	-0.035
²⁴⁴ Bk	6.779	6.724	0.055
²⁴⁵ Bk	6.455	6.419	0.036
²⁴⁶ Bk	6.074	6.149	-0.075
²⁴⁷ Bk	5.890	5.896	-0.006
²⁴⁸ Bk	5.827	5.765	0.062
²⁴⁹ Bk	5.521	5.610	-0.089
²³⁷ Cf	8.220	8.249	-0.029
²³⁹ Cf	7.763	7.886	-0.123
²⁴⁰ Cf	7.711	7.745	-0.034
²⁴² Cf	7.517	7.541	-0.024
²⁴⁴ Cf	7.329	7.337	-0.008
²⁴⁵ Cf	7.258	7.169	0.089
²⁴⁶ Cf	6.862	6.862	0.000
²⁴⁷ Cf	6.503	6.585	-0.082
²⁴⁸ Cf	6.361	6.358	0.003
²⁴⁹ Cf	6.293	6.263	0.030
²⁵⁰ Cf	6.129	6.174	-0.045
²⁵¹ Cf	6.177	6.175	0.002
²⁵² Cf	6.217	6.166	0.051
²⁵³ Cf	6.126	6.166	-0.040
²⁵⁴ Cf	5.927	5.915	0.012
²⁴¹ Es	8.259	8.336	-0.077
²⁴² Es	8.160	8.062	0.098
²⁴³ Es	8.072	7.905	0.167
²⁴⁵ Es	7.909	7.610	0.299
²⁴⁷ Es	7.464	7.378	0.086
²⁵¹ Es	6.597	6.709	-0.112
²⁵² Es	6.739	6.702	0.037
²⁵³ Es	6.739	6.683	0.056
²⁵⁴ Es	6.617	6.676	-0.059
²⁵⁵ Es	6.436	6.415	0.021
²⁴³ Fm	8.689	9.127	-0.438
²⁴⁶ Fm	8.379	8.391	-0.012
²⁴⁷ Fm	8.258	8.105	0.153
²⁴⁸ Fm	7.995	7.980	0.015
²⁴⁹ Fm	7.709	7.713	-0.004
²⁵⁰ Fm	7.557	7.563	-0.006
²⁵¹ Fm	7.424	7.359	0.065
²⁵² Fm	7.154	7.255	-0.101
²⁵³ Fm	7.198	7.192	0.006

Table 1: (continued)

Nucl.	$Q_{\alpha}^{\text{Expt.}}$ (MeV)	$Q_{\alpha}^{\text{Theo.}}$ (MeV)	ΔQ_{α} (MeV)
²⁵⁴ Fm	7.307	7.256	0.051
²⁵⁵ Fm	7.241	7.259	-0.018
²⁵⁶ Fm	7.025	7.032	-0.007
²⁵⁷ Fm	6.864	6.882	-0.018
²⁴⁶ Md	8.889	9.193	-0.304
²⁴⁷ Md	8.764	8.983	-0.219
²⁴⁸ Md	8.497	8.647	-0.150
²⁵⁰ Md	8.155	8.135	0.020
²⁵¹ Md	7.963	7.982	-0.019
²⁵³ Md	7.573	7.814	-0.241
²⁵⁵ Md	7.906	7.834	0.072
²⁵⁷ Md	7.557	7.505	0.052
²⁵⁸ Md	7.271	7.263	0.008
²⁵¹ No	8.752	8.833	-0.081
²⁵² No	8.549	8.555	-0.006
²⁵³ No	8.415	8.406	0.009
²⁵⁴ No	8.226	8.327	-0.101
²⁵⁵ No	8.428	8.413	0.015
²⁵⁶ No	8.582	8.480	0.102
²⁵⁷ No	8.477	8.496	-0.019
²⁵⁹ No	7.854	7.859	-0.005

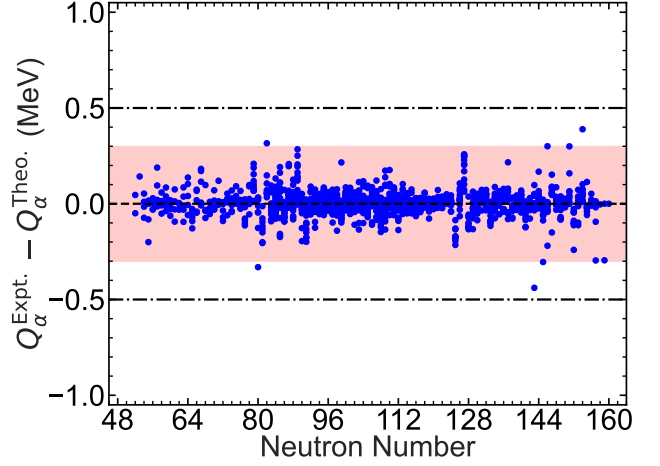


Fig. 3. The deviations between the experimental α -decay energies and the theoretical results for 1169 nuclei with $50 \leq Z \leq 110$. The blue circles depict the deviations for these nuclei. The dashed line denotes $|Q_{\alpha}^{\text{Expt.}} - Q_{\alpha}^{\text{Theo.}}| = 0$ MeV. The red shadow and the dash dotted lines present $|Q_{\alpha}^{\text{Expt.}} - Q_{\alpha}^{\text{Theo.}}| \leq 0.3$ MeV and $|Q_{\alpha}^{\text{Expt.}} - Q_{\alpha}^{\text{Theo.}}| \leq 0.5$ MeV, respectively.

given by

$$\langle \sigma_{\alpha} \rangle = \frac{1}{\tilde{n}_{\alpha}} \sum_{p=1}^{\tilde{n}_{\alpha}} |Q_{\alpha}^{\text{Expt.},p} - Q_{\alpha}^{\text{Theo.},p}| = 0.047 \text{ MeV} \quad (7)$$

and

$$\sqrt{\sigma_{\alpha}^2} = \sqrt{\frac{1}{\tilde{n}_{\alpha}} \sum_{p=1}^{\tilde{n}_{\alpha}} (Q_{\alpha}^{\text{Expt.},p} - Q_{\alpha}^{\text{Theo.},p})^2} = 0.070 \text{ MeV}. \quad (8)$$

Owing to the complexity of the quantum many-body theory, it is difficult to calculate the α -decay energies with deviations less than 0.1 MeV. These small deviations show that the α -decay energies agree well with the experimental results.

Recently, some actinide nuclei, including ²⁰⁴Ac [57] and ²⁰⁷Th [10], were synthesized experimentally. Theoretical α -decay properties provide useful references for these experiments. Here, we present the theoretical α -decay energies calculated using the Gaussian process for the actinide nuclei in Table 1. In Table 1, the first column lists the actinide nuclei. The second column denotes the experimental data and the third column presents the theoretical results. The fourth column gives the deviations $\Delta Q_{\alpha} = Q_{\alpha}^{\text{Expt.}} - Q_{\alpha}^{\text{Theo.}}$ between the experimental results and the theoretical ones. The experimental α -decay energies for two new nuclides ²⁰⁴Ac and ²⁰⁷Th are taken from Ref. [57] and Ref. [10] separately. It can be clearly seen that the theoretical results obtained using the Gaussian process are in good agreement with the experimental data for the actinide nuclei. For the new nuclide ²⁰⁴Ac, the theoretical α -decay energy calculated using the Gaussian process is nearly equivalent to the experimental result, with a small deviation of $\Delta Q_{\alpha} = Q_{\alpha}^{\text{Expt.}} - Q_{\alpha}^{\text{Theo.}} = 0.0004$ MeV. For another new nuclide, ²⁰⁷Th, the deviation is

Due to the successful calculations of the binding energies, it is expected that the α -decay energies, which are the differences among the binding energies of the parent nuclei, the daughter nuclei, and the α -particles, can be reproduced with good accuracy. Thus, we calculate the α -decay energies for 1169 nuclei with $50 \leq Z \leq 110$ and compare the calculated results with the experimental data taken from AME2020 [27]. The deviations between the experimental α -decay energies and the theoretical results for these nuclei are depicted in Fig. 3. In Fig. 3, the blue circles denote the deviations and the red shadow shows the deviations $|Q_{\alpha}^{\text{Expt.}} - Q_{\alpha}^{\text{Theo.}}| \leq 0.3$ MeV. The dashed line represents $|Q_{\alpha}^{\text{Expt.}} - Q_{\alpha}^{\text{Theo.}}| = 0$ MeV and the two dash dotted lines present $|Q_{\alpha}^{\text{Expt.}} - Q_{\alpha}^{\text{Theo.}}| = 0.5$ MeV, respectively. The deviations for the α -decay energies of the 1169 nuclei are all clearly below 0.5 MeV and the deviations for most of these nuclei are less than 0.3 MeV. These results show good agreement between the theoretical α -decay energies derived from the binding energies which are calculated using the Gaussian process and the experimental data. Furthermore, it has been found in previous studies that α -decay energies are strongly affected by the shell effect, which leads to larger deviations for nuclei near the closed shell [56]. In Fig. 3, the deviations for nuclei near the shell closure are also less than 0.3 MeV. It can reflect that π and ν features can successfully model the shell effect with the Gaussian process. We also calculate the average deviation and standard deviation for these nuclei,

$\Delta Q_\alpha = Q_\alpha^{\text{Expt.}} - Q_\alpha^{\text{Theo.}} = 0.051 \text{ MeV}$, indicating that the calculated result is in good agreement with the experimental one. These results demonstrate that the α -decay energies for the actinide nuclei can be well reproduced by deriving from the theoretical binding energies calculated using the Gaussian process. Overall, the above results show the reliability of the Gaussian process in the calculations of nuclear binding energies and α -decay properties.

Table 2: The predicted α -decay energies and half-lives for some unknown actinide nuclei. The first column denotes the α -decay emitters. The second and third columns are the predicted α -decay energies calculated using the Gaussian process and the FRDM separately. The fourth and fifth columns represent the predicted α -decay half-lives calculated using the NGNL with the predicted α -decay energies given by the Gaussian process and the FRDM, respectively. The units of the α -decay half-lives are seconds.

Nucl.	Q_α^{GP} (MeV)	Q_α^{FRDM} (MeV)	$\log_{10}(T_{1/2}^{\text{GP}})$	$\log_{10}(T_{1/2}^{\text{FRDM}})$
^{200}Ac	9.260	8.905	-4.982	-4.089
^{201}Ac	9.016	8.895	-4.373	-4.062
^{202}Ac	8.639	8.685	-3.383	-3.507
^{203}Ac	8.432	8.575	-2.811	-3.208
^{203}Th	8.948	8.825	-3.865	-3.542
^{204}Th	8.827	8.765	-3.547	-3.381
^{205}Th	8.595	8.575	-2.917	-2.862
^{206}Th	8.469	8.515	-2.565	-2.694
^{207}Pa	8.495	8.765	-2.289	-3.040
^{208}Pa	8.478	8.565	-2.240	-2.487
^{209}Pa	8.461	8.305	-2.191	-1.738
^{210}Pa	8.456	8.265	-2.176	-1.619
^{210}U	8.456	8.605	-1.825	-2.252
^{211}U	8.512	8.485	-1.986	-1.909
^{212}U	8.490	8.365	-1.922	-1.558
^{213}U	8.542	8.385	-2.071	-1.617
^{215}Np	8.444	8.815	-1.435	-2.490
^{216}Np	8.544	8.625	-1.726	-1.958
^{217}Np	8.684	8.725	-2.124	-2.239
^{218}Np	8.956	8.945	-2.872	-2.842
^{224}Pu	9.914	9.565	-5.944	-5.107
^{225}Pu	9.306	9.285	-4.455	-4.401
^{226}Pu	8.774	9.035	-3.028	-3.744
^{227}Pu	8.246	8.695	-1.476	-2.804
^{225}Am	9.977	9.895	-5.779	-5.587
^{226}Am	9.348	9.605	-4.235	-4.884
^{227}Am	8.936	9.345	-3.136	-4.227
^{228}Am	8.423	9.075	-1.657	-3.515
^{229}Cm	8.727	9.395	-2.202	-4.027
^{230}Cm	8.419	8.725	-1.288	-2.196
^{231}Cm	8.068	8.385	-0.182	-1.183

Table 2: (continued)

Nucl.	Q_α^{GP} (MeV)	Q_α^{FRDM} (MeV)	$\log_{10}(T_{1/2}^{\text{GP}})$	$\log_{10}(T_{1/2}^{\text{FRDM}})$
^{232}Cm	7.788	7.885	0.753	0.424
^{229}Bk	9.233	9.555	-3.270	-4.112
^{230}Bk	8.864	9.165	-2.249	-3.086
^{231}Bk	8.549	8.805	-1.326	-2.080
^{232}Bk	8.270	8.465	-0.464	-1.070
^{233}Cf	9.392	8.585	-3.360	-1.080
^{234}Cf	9.092	8.665	-2.548	-1.319
^{235}Cf	8.726	8.535	-1.500	-0.927
^{236}Cf	8.509	8.335	-0.847	-0.305
^{237}Es	9.679	8.645	-3.778	-0.906
^{238}Es	9.215	8.485	-2.548	-0.415
^{239}Es	8.935	8.155	-1.760	0.643
^{240}Es	8.558	7.975	-0.639	1.248
^{239}Fm	10.540	8.845	-5.536	-1.152
^{240}Fm	10.260	8.605	-4.887	-0.428
^{241}Fm	9.791	8.405	-3.739	0.199
^{242}Fm	9.548	8.285	-3.110	0.586
^{242}Md	10.392	9.045	-4.889	-1.389
^{243}Md	10.139	9.005	-4.284	-1.273
^{244}Md	9.767	8.935	-3.354	-1.068
^{245}Md	9.541	8.925	-2.762	-1.038
^{245}No	10.326	9.505	-4.423	-2.336
^{246}No	10.104	9.465	-3.883	-2.227
^{247}No	9.878	9.335	-3.316	-1.869
^{248}No	9.629	9.205	-2.667	-1.504

Finally, we predict the α -decay energies for some unknown actinide nuclei using the Gaussian process. With the predicted α -decay energies, we also calculate the α -decay half-lives using the new Geiger-Nuttall law (NGNL) [58]. The corresponding results are given in Table 2. In Table 2, the first column lists the α -emitters. The second and third columns present the α -decay energies calculated using the Gaussian process and the FRDM, respectively. The fourth and fifth columns give the predictive α -decay half-lives calculated using the NGNL with the α -decay energies predicted by the Gaussian process and the FRDM, respectively. It can be found that most predicted α -decay energies agree well with those calculated using the FRDM. Nevertheless, the predicted α -decay energies for Einsteinium, Fermium, Mendelevium, and Nobelium are relatively larger than those given by the FRDM, which results in different α -decay half-lives. We hope that future experimental α -decay properties for Einsteinium, Fermium, Mendelevium, and Nobelium can provide useful information for improving the Gaussian process. The α -decay properties predicted by the Gaussian process can complement existing theoretical models and provide valuable guidance for future studies of α decay. In addition, some ac-

tinide isotopes are being synthesized at the Heavy Ion Research Facility in Lanzhou (HIRFL), China. Therefore, it is expected that the predicted α -decay properties can be used as theoretical references for identifying new nuclides in the future.

IV. SUMMARY

In this work, the Gaussian process with a composite kernel function is applied to study the binding energies. First, we calculate the binding energies for 2238 nuclei with $Z > 20$ and $N > 20$ within the framework of the Gaussian process using a physically motivated feature space. The calculated average deviation and standard deviation are 0.046 MeV and 0.066 MeV, respectively. The results demonstrate that the binding energies are successfully modeled by the Gaussian process, reflecting the good learning ability of the Gaussian process in the calculations of binding energies. Then, we cal-

culate the binding energies for 108 nuclei, which are newly included in AME2020. The calculated results are in good agreement with the experimental data, which indicates the good predictive power of the Gaussian process in the studies of binding energies. Moreover, the application of the composite kernel function provides a novel perspective in studying other physical problems using the Gaussian process. Next, we calculate the α -decay energies due to the successful calculations of the binding energies using the Gaussian process. The average deviation and the standard deviation for 1169 nuclei with $50 \leq Z \leq 110$ are 0.047 MeV and 0.070 MeV, respectively. Notably, the theoretical α -decay energies for the new nuclides ^{204}Ac and ^{207}Th are well reproduced with $\Delta Q_\alpha = 0.0004$ MeV for ^{204}Ac and $\Delta Q_\alpha = 0.051$ MeV for ^{207}Th . The good results also show that the Gaussian process is reliable for the studies of binding energies. Finally, the α -decay properties for the actinide nuclei are predicted using the Gaussian process. We expect the predicted results will be useful for future studies of the binding energies and the α -decay properties.

-
- [1] W. D. Myers and W. J. Swiatecki, Nuclear masses and deformations, Nucl. Phys. **81**, 1-60 (1966). doi:10.1016/S0029-5582(66)80001-9
- [2] W. Mittig, A. Lepine-Szily, and N. A. Orr, Mass measurement far from stability, Ann. Rev. Nucl. Part. Sci. **47**, 27-66 (1997). doi:10.1146/annurev.nucl.47.1.27
- [3] Z. Ren, F. Tai, and D. H. Chen, Systematic calculations of the ground state properties of superheavy nuclei, Phys. Rev. C **66**, 064306 (2002). doi:10.1103/PhysRevC.66.064306
- [4] D. Lunney, J. M. Pearson, and C. Thibault, Recent trends in the determination of nuclear masses, Rev. Mod. Phys. **75**, 1021-1082 (2003). doi:10.1103/RevModPhys.75.1021
- [5] M. E. Burbidge, G. R. Burbidge, W. A. Fowler *et al.*, Synthesis of the elements in stars, Rev. Mod. Phys. **29**, 547-650 (1957). doi:10.1103/RevModPhys.29.547
- [6] S. Hofmann and G. Munzenberg, The discovery of the heaviest elements, Rev. Mod. Phys. **72**, 733-767 (2000). doi:10.1103/RevModPhys.72.733
- [7] T. Dong and Z. Ren, New model of binding energies of heavy nuclei with $Z \geq 90$, Phys. Rev. C **72**, 064331 (2005). doi:10.1103/PhysRevC.72.064331
- [8] T. Dong and Z. Ren, Improved version of a binding energy formula for heavy and superheavy nuclei with $Z \geq 90$ and $N \geq 140$, Phys. Rev. C **77**, 064310 (2008). doi:10.1103/PhysRevC.77.064310
- [9] Z. Y. Zhang, H. B. Yang, M. H. Huang *et al.*, New α -emitting isotope ^{214}U and abnormal enhancement of α -particle clustering in lightest Uranium isotopes, Phys. Rev. Lett. **126**, 152502 (2021). doi:10.1103/PhysRevLett.126.152502
- [10] H. B. Yang, Z. G. Gan, Z. Y. Zhang *et al.*, New isotope ^{207}Th and odd-even staggering in α -decay energies for nuclei with $Z > 82$ and $N < 126$, Phys. Rev. C **105**, L051302 (2022). doi:10.1103/PhysRevC.105.L051302
- [11] C. Qi, R. Liotta, and R. Wyss, Recent developments in radioactive charged-particle emissions and related phenomena, Prog. Part. Nucl. Phys. **105**, 214 (2019). doi:10.1016/j.pnpnp.2018.11.003
- [12] D. S. Delion, Z. Ren, A. Dumitrescu *et al.*, Coupled channels description of the α -decay fine structure, J. Phys. G: Nucl. Part. Phys. **45**, 053001 (2018). doi:10.1088/1361-6471/aaac52
- [13] Z. Wang, Z. Ren, Predictions of the decay properties of the superheavy nuclei $^{293,294}119$ and $^{294,295}120$, Nucl. Tech. **46**, 114-120 (2023). doi:10.11889/j.0253-3219.2023.hjs.46.080011
- [14] D. Bai and Z. Ren, α clustering slightly above ^{100}Sn in the light of the new experimental data on the superallowed α decay, Eur. Phys. J. A **54**, 220 (2018). doi:10.1140/epja/i2018-12673-4
- [15] D. Bai, Z. Ren, and G. Röpke, α clustering from the quartet model, Phys. Rev. C **99**, 034305 (2019). doi:10.1103/PhysRevC.99.034305
- [16] Z. Wang, D. Bai and Z. Ren, Improved density-dependent cluster model in α -decay calculations within anisotropic deformation-dependent surface diffuseness, Phys. Rev. C **105**, 024327 (2022). doi:10.1103/PhysRevC.105.024327
- [17] Z. Wang and Z. Ren, Favored α -decay half-lives of odd- A and odd-odd nuclei using an improved density-dependent cluster model with anisotropic surface diffuseness, Phys. Rev. C **106**, 024311 (2022). doi:10.1103/PhysRevC.106.024311
- [18] J. Liu, Z. Wang, H. Zhang *et al.*, Theoretical predictions on cluster radioactivity of superheavy nuclei with $Z = 119, 120$, Chin. Phys. C **48**, 014105 (2024). doi:10.1088/1674-1137/ad0827
- [19] Z. Yuan, D. Bai, Z. Wang *et al.*, Research on two-proton radioactivity in density-dependent cluster model, Sci. China Phys. Mech. Astron. **66**, 222012 (2023). doi:10.1007/s11433-022-1994-8
- [20] Z. Ren, C. Xu, and Z. Wang, New perspective on complex cluster radioactivity of heavy nuclei, Phys. Rev. C **70**, 034304 (2004). doi:10.1103/PhysRevC.70.034304
- [21] M. Arnould, S. Goriely, and K. Takahashi, The r -process of stellar nucleosynthesis: Astrophysics and nuclear physics achievements and mysteries, Phys. Rept. **450**, 97-213 (2007). doi:10.1016/j.physrep.2007.06.002
- [22] M. R. Mumpower, R. Surman, G. C. McLaughlin *et al.*, The impact of individual nuclear properties on r -process nu-

- cleosynthesis, *Prog. Part. Nucl. Phys.* **86**, 86-126 (2016).
doi:10.1016/j.pnpnp.2015.09.001
- [23] R. R. C. Clement, W. Benenson, B. A. Brown *et al.*, Sensitivities of rp -process calculations to nuclear mass uncertainties, *Nucl. Phys. A* **718**, 617-619 (2003). doi:10.1016/S0375-9474(03)00903-5
- [24] E. Haettner, D. Ackermann, G. Audi *et al.*, Mass measurements of very neutron-deficient Mo and Tc isotopes and their impact on rp process nucleosynthesis, *Phys. Rev. Lett.* **106**, 122501 (2011). doi:10.1103/PhysRevLett.106.122501
- [25] M. Oertel, M. Hempel, T. Klöhn *et al.*, Equations of state for supernovae and compact stars, *Rev. Mod. Phys.* **89**, 015007 (2017). doi:10.1103/RevModPhys.89.015007
- [26] B. Hong and Z. Ren, Mixed dark matter models for the peculiar compact object in remnant HESS J1731-347 and their implications for gravitational wave properties, *Phys. Rev. D* **109**, 023002 (2024). doi:10.1103/PhysRevD.109.023002
- [27] M. Wang, W. J. Huang, F. G. Kondev *et al.*, The AME 2020 atomic mass evaluation (II). Tables, graphs and references, *Chin. Phys. C* **45**, 030003 (2021). doi:10.1088/1674-1137/abddaf
- [28] C. F. von Weizsäcker, Zur theorie der Kernmassen, *Z. Phys.* **96**, 431-458 (1935). doi:10.1007/BF01337700
- [29] H. A. Bethe and R. F. Bacher, Nuclear physics A. Stationary states of nuclei, *Rev. Mod. Phys.* **8**, 82-229 (1936). doi:10.1103/RevModPhys.8.82
- [30] W. D. Myers and W. J. Swiatecki, Nuclear properties according to the Thomas-Fermi model, *Nucl. Phys. A* **601**, 141-167 (1996). doi:10.1016/0375-9474(95)00509-9
- [31] S. Goriely, S. Hilaire, M. Girod *et al.*, First Gogny-Hartree-Fock-Bogoliubov nuclear mass model, *Phys. Rev. Lett.* **102**, 242501 (2009). doi:10.1103/PhysRevLett.102.242501
- [32] P. Möller, A. J. Sierk, T. Ichikawa *et al.*, Nuclear ground-state masses and deformations: FRDM(2012), *Atom. Data Nucl. Data Tabl.* **109-110**, 1-204 (2016). doi:10.1016/j.adt.2015.10.002
- [33] G. Carleo, I. Cirac, K. Cranmer *et al.*, Machine learning and the physical sciences, *Rev. Mod. Phys.* **91**, 045002 (2019). doi:10.1103/RevModPhys.91.045002
- [34] A. Boehnlein, M. Diefenthaler, N. Sato *et al.*, Colloquium: Machine learning in nuclear physics, *Rev. Mod. Phys.* **94**, 031003 (2022). doi:10.1103/RevModPhys.94.031003
- [35] W. He, Q. Li, Y. Ma *et al.*, Machine learning in nuclear physics at low and intermediate energies, *Sci. China Phys. Mech. Astron.* **66**, 282001 (2023). doi:10.1007/s11433-023-2116-0
- [36] W. B. He, Y. G. Ma, L. G. Pang *et al.*, High-energy nuclear physics meets machine learning, *Nucl. Sci. Tech.* **34**, 88 (2023). doi:10.1007/s41365-023-01233-z
- [37] Z. X. Yang, X. H. Fan, P. Yin *et al.*, Taming nucleon density distributions with deep neural network, *Phys. Lett. B* **823**, 136650 (2021). doi:10.1016/j.physletb.2021.136650
- [38] C. W. Ma, X. X. Chen, X. B. Wei *et al.*, Systematic behavior of fragments in Bayesian neural network models for projectile fragmentation reactions, *Phys. Rev. C* **108**, 044606 (2023). doi:10.1103/PhysRevC.108.044606
- [39] Z. M. Niu and H. Z. Liang, Nuclear mass predictions based on Bayesian neural network approach with pairing and shell effects, *Phys. Lett. B* **778**, 48 (2018). doi:10.1016/j.physletb.2018.01.002
- [40] Z. Gao, Y. Wang, H. Lü *et al.*, Machine learning the nuclear mass, *Nucl. Sci. Tech.* **32**, 109 (2021). doi: 10.1007/s41365-021-00956-1
- [41] A. E. Lovell, A. T. Mohan, T. M. Sprouse *et al.*, Nuclear masses learned from a probabilistic neural network, *Phys. Rev. C* **106**, 014305 (2022). doi:10.1103/PhysRevC.106.014305
- [42] Y. Ma, C. Su, J. Liu *et al.*, Predictions of nuclear charge radii and physical interpretations based on the naive Bayesian probability classifier, *Phys. Rev. C* **101**, 014304 (2020). doi:10.1103/PhysRevC.101.014304
- [43] G. Saxena, P. K. Sharma, and P. Saxena, Modified empirical formulas and machine learning for α -decay systematics, *J. Phys. G: Nucl. Part. Phys.* **48**, 055103 (2021). doi:10.1088/1361-6471/abcd1c
- [44] Z. M. Niu, H. Z. Liang, B. H. Sun *et al.*, Predictions of nuclear β -decay half-lives with machine learning and their impact on r -process nucleosynthesis, *Phys. Rev. C* **99**, 064307 (2019). doi:10.1103/PhysRevC.99.064307
- [45] Z. M. Niu and H. Z. Liang, Nuclear mass predictions with machine learning reaching the accuracy required by r -process studies, *Phys. Rev. C* **106**, L021303 (2022). doi:10.1103/PhysRevC.106.L021303
- [46] C. Rasmussen and C. Williams, Gaussian Processes for Machine Learning. [GaussianProcess.org](https://gaussianprocess.org)
- [47] A. Hanuka, X. Huang, J. Shtalenkova, *et al.* Physics model-informed Gaussian process for online optimization of particle accelerators, *Phys. Rev. Accel. Beams* **24**, 072802 (2021). doi:10.1103/PhysRevAccelBeams.24.072802
- [48] J. Cui and R. V. Krems, Gaussian process model for collision dynamics of complex molecules, *Phys. Rev. Lett.* **115**, 073202 (2015). doi:10.1103/PhysRevLett.115.073202
- [49] D. Wee, J. Kim, S. Bang *et al.*, Quantification of uncertainties in thermoelectric properties of materials from a first-principles prediction method: An approach based on Gaussian process regression, *Phys. Rev. Materials* **3**, 033803 (2019). doi:10.1103/PhysRevMaterials.3.033803
- [50] Z. Yuan, D. Bai, Z. Ren *et al.*, Theoretical predictions on α -decay properties of some unknown neutron-deficient actinide nuclei using machine learning, *Chin. Phys. C* **46**, 024101 (2022). doi:10.1088/1674-1137/ac321c
- [51] Z. Zhao, J. K. Fitzsimons, and J. F. Fitzsimons, Quantum-assisted Gaussian process regression, *Phys. Rev. A* **99**, 052331 (2019). doi:10.1103/PhysRevA.99.052331
- [52] A. Bohr and B. R. Mottelson, *Nuclear Structure Vol. 1: Single-Particle Motion* (World Scientific, Singapore, 1998).
- [53] J. Lilley, *Nuclear Physics: Principles and Applications* (Wiley, Chichester, 2002).
- [54] M. W. Kirson, Mutual influence of terms in a semi-empirical mass formula, *Nucl. Phys. A* **798**, 29-60 (2008). doi:10.1016/j.nuclphysa.2007.10.011
- [55] F. G. Kondev, M. Wang, W. J. Huang *et al.*, The NUBASE2020 evaluation of nuclear physics properties, *Chin. Phys. C* **45**, 030001 (2021). doi:10.1088/1674-1137/abddae
- [56] T. Dong and Z. Ren, α -decay energy formula for superheavy nuclei based on the liquid-drop model, *Phys. Rev. C* **82**, 034320 (2010). doi:10.1103/PhysRevC.82.034320
- [57] M. H. Huang, Z. G. Gan, Z. Y. Zhang *et al.*, α decay of the new isotope ^{204}Ac , *Phys. Lett. B* **834**, 137484 (2022). doi:10.1016/j.physletb.2022.137484
- [58] Y. Ren and Z. Ren, New Geiger-Nuttall law for α decay of heavy nuclei, *Phys. Rev. C* **85**, 044608 (2012). doi:10.1103/PhysRevC.85.044608